Shear-stress relaxation in free-standing polymer films

G. George,[1] I. Kriuchevskyi,[2] H. Meyer,[1] J. Baschnagel,[1] and J. P. Wittmer[1,*]

[1]*Institut Charles Sadron, Université de Strasbourg & CNRS, 23 rue du Loess, 67034 Strasbourg Cedex, France*
[2]*LAMCOS, INSA, 27 avenue Jean Capelle, 69621 Villeurbanne Cedex, France*

Using molecular dynamics simulation of a polymer glass model we investigate free-standing polymer films focusing on the in-plane shear modulus μ, defined by means of the stress-fluctuation formula, as a function of temperature T, film thickness H (tuned by means of the lateral box size L), and sampling time Δt. Various observables are seen to vary linearly with $1/H$, demonstrating thus the (to leading order) linear superposition of bulk and surface properties. Confirming the time-translational invariance of our systems, $\mu(\Delta t)$ is shown to be numerically equivalent to a second integral over the shear-stress relaxation modulus $G(t)$. It is thus a natural smoothing function statistically better behaved as $G(t)$. As shown from the standard deviations $\delta\mu$ and δG, this is especially important for large times and for temperatures around the glass transition. μ and G are found to decrease continuously with T and a jump-singularity is not observed. Using the Einstein-Helfand relation for $\mu(\Delta t)$ and the successful time-temperature superposition scaling of $\mu(\Delta t)$ and $G(t)$, the shear viscosity $\eta(T)$ can be estimated for a broad range of temperatures.

I. INTRODUCTION

A. Generalized shear modulus $\mu(\Delta t)$

An important mechanical property characterizing elastic solids or more general viscoelastic bodies is the thermodynamic equilibrium shear modulus μ_{eq} [1,2]. (We remind that $\mu_{\mathrm{eq}} = 0$ for simple or complex liquids.) As sketched in Fig. 1, μ_{eq} is the long-time limit of the shear-stress relaxation modulus $G(t)$, i.e., the ratio of the measured shear stress $\sigma(t)$ and the imposed (infinitesimal) simple shear strain γ. Instead of using a tedious out-of-equilibrium simulation tilting the simulation box as shown in Fig. 1(a), the shear modulus may be conveniently obtained numerically using equilibrium time series of the instantaneous shear stress $\hat{\sigma}$ and the instantaneous affine shear modulus $\hat{\mu}_{\mathrm{A}}$ as defined in Appendix A 2. This is done by means of the well-known stress-fluctuation formula [3–14]

$$\mu(\Delta t) \equiv \mu_{\mathrm{A}} - \mu_{\mathrm{F}}(\Delta t) \quad \text{with} \quad \mu(\Delta t) \to \mu_{\mathrm{eq}}, \quad (1)$$

in the limit of a sufficiently large sampling time Δt of the computer experiment [15]. As sketched in Fig. 1(b), the "affine shear modulus" μ_{A} describes the elastic response assuming an infinitesimal canonical affine strain (Appendix A 1) of all parts of the body under the macroscopic simple shear constraint. Correcting the resulting overestimation of the modulus, the nonaffine contribution $\mu_{\mathrm{F}}(\Delta t)$ measures the fluctuations of $\hat{\sigma}$. (For details see Sec. III B.) The indicated Δt-dependencies naturally arise since the averages for μ_{A} and μ_{F} are commonly and most conveniently done by first "time-averaging" over time windows of length Δt of the stored data entries of a given configuration and only in a second step

by "ensemble-averaging" over completely independent configurations (Appendix B 2). Assuming the time-translational invariance of the time series it can be demonstrated (Appendix C) that the Δt-dependence can be traced back to the stationarity relation [9,11,14]

$$\mu(\Delta t) = \frac{2}{\Delta t^2} \int_0^{\Delta t} dt \int_0^t dt' \, G(t'). \quad (2)$$

Being a second integral over $G(t)$, $\mu(\Delta t)$ is a convenient smoothing function with in general much better statistical properties as $G(t)$. The historically thermodynamically rooted stress-fluctuation formula, Eq. (1), takes due to Eq. (2) the meaning of a generalized quasi-static modulus also containing information about dissipation processes associated with the reorganization of the particle contact network. This has been extensively tested for self-assembled transient networks [11].

B. Shear modulus of glass-forming systems

The (thermodynamically well-defined) shear modulus $\mu_{\mathrm{eq}}(T)$ of crystalline solids is known to vanish discontinuously at the melting point with increasing temperature T [4,12]. This begs the question of whether μ_{eq} or a natural generalization, such as $\mu(\Delta t)$ describing also stationary out-of-equilibrium systems and general viscoelastic bodies, behave similarly for amorphous glass-forming colloids or polymers at their glass transition temperature T_{g} [4,6,8,12–14,16–22]. Qualitative different theoretical [17–19,22], experimental [20,21], or numerical [4,8,13,14] findings have been put forward suggesting either a *discontinuous jump* [16,17,19–21] or a *continuous* transition [4,8,12–14,18,22]. Following the pioneering work of Barrat *et al.* [4] various numerical studies have used the stress-fluctuation formula, Eq. (1), as the main diagnostic tool to characterize the shear strain response [4,6,8,12–14]. Using molecular dynamics (MD) simulation

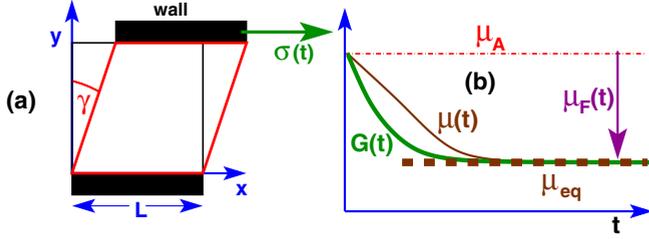_____

*joachim.wittmer@ics-cnrs.unistra.fr

FIG. 1. Some notations: (a) Simple shear with γ being the strain increment imposed at $t = 0$ and $\sigma(t)$ the measured shear stress increment as a function of time t. (b) Shear-stress relaxation modulus $G(t)$ (dash-dotted line) and generalized shear modulus $\mu(t) = \mu_A - \mu_F(t)$ (thin solid line). The *affine* shear modulus $\mu_A = G(t = 0) = \mu(t = 0)$ is indicated by the dash-dotted line, the thermodynamic long-time limit μ_{eq} for $G(t)$ and $\mu(t)$ by the bold dashed line.

[23,24] of a coarse-grained bead-spring model [6,13,14,25], we have recently investigated $\mu(\Delta t)$ and $G(t)$ for three-dimensional (3D) polymer melts [13,14]. The most important findings are that

(1) the stationarity relation Eq. (2) holds for all temperatures, i.e., the expectation values of $\mu(\Delta t)$ and $G(t)$ are numerically equivalent;

(2) this is not the case for their standard deviations $\delta\mu$ and δG for which $\delta\mu(T) \ll \delta G(T)$ holds;

(3) if taken at the same (sampling) time, $\mu(T)$ and $G(T)$ are found to decrease continuously with T;

(4) $\delta\mu(T)$ and $\delta G(T)$ are nonmonotonic with strong peaks slightly below T_g. Theoretical calculations for the expectation values of an ensemble of independent configurations are thus largely irrelevant for predicting the behavior of one configuration.

C. Aim of present study

As sketched in Fig. 2, the present study extends our previous work to free-standing polymer films of finite thickness H tuned by means of the imposed lateral box size L. It is well
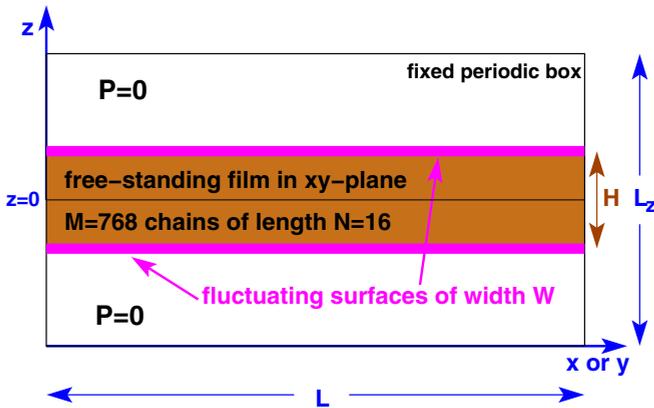

FIG. 2. We study free-standing polymer films with $M = 768$ chains of length $N = 16$ monomers confined in periodic boxes with L being the imposed lateral box size in both x and y directions. The film thickness $H \sim 1/L^2$ (to leading order) is operationally defined using the Gibbs dividing surface.
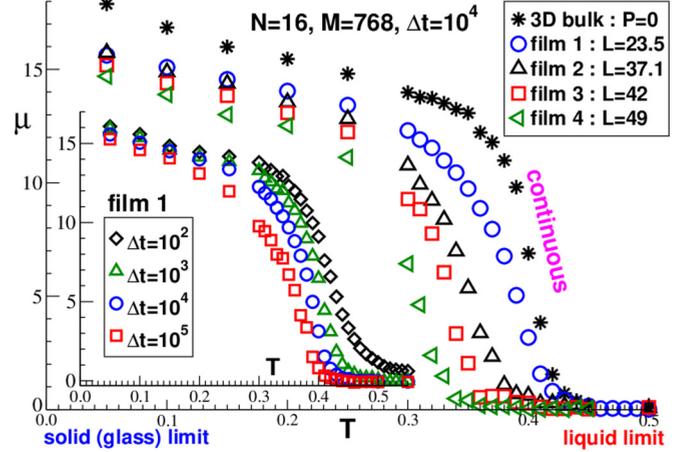

FIG. 3. Shear modulus μ as calculated by means of Eq. (1). $\mu(T)$ decays continuously in all cases considered. Main panel: Data obtained at a sampling time $\Delta t = 10^4$ for three-dimensional bulks (stars) and films of different lateral box lengths L. Inset: $\mu(T)$ for film 1 comparing different Δt.

known that the confinement of polymers to thin films can dramatically change their physical properties [26–66]. Substantial efforts have been made experimentally [26–29,31,32], numerically [52,53,56–58,62,64,65], and theoretically [44–50] to describe the glass transition temperature showing as a general trend that free surfaces lead to a decrease of T_g [66]. Despite their technological importance, mechanical and rheological properties have been much less studied experimentally [34,36,37,40,66,67]. (One reason is that much smaller and more precise load cells are required due to the tiny loads needed to deform the films [66].) Perhaps as a consequence, only a small number of numerical studies exist at present focusing on the mechanical properties of films [55,58–61,63,65] and related amorphous polymer nanostructures [58]. Attempting to fill this gap and using the same coarse-grained numerical model as in Refs. [6,13,14], we focus here on the in-plane shear-stresses, their fluctuations, and relaxation dynamics. At variance to real experiments [34,36,37,40,67], we use again as the main diagnostic tool the first time-averaged and then ensemble-averaged generalized shear modulus μ and its various contributions as defined by the stress-fluctuation formula, Eq. (1). Only total film properties will be discussed for clarity; their z-resolved contributions will be given elsewhere.

D. Some key findings

Summarizing several points made in this paper, we present $\mu(T)$ in Fig. 3 for different systems (main panel) and sampling times Δt (inset). As explained in Appendix B 1, Lennard-Jones (LJ) units [23] are used here as everywhere in this work. Confirming our recent work on 3D melts, $\mu(T)$ is observed to decay *continuously* in all cases. Also, as emphasized in the inset, μ systematically depends on Δt. In addition, it is seen in the main panel that μ becomes finite at lower temperatures for thinner films (larger L). We corroborate these findings in the remainder of this paper. Importantly, Eq. (2) will be demonstrated to hold also for polymer films and $\mu(\Delta t)$ is thus a natural smoothing function with much better

statistics as $G(t)$. As shown from the standard deviations $\delta\mu$ and δG, this is especially important for large times and for temperatures around the glass transition. Using the successful time-temperature superposition (TTS) of $\mu(\Delta t)$ and $G(t)$ it will be shown that the shear viscosity $\eta(T)$ can be estimated for a broad range of temperatures.

Many intensive properties $\mathcal{A}$, such as T_g, μ_A or μ_F, will be seen to depend linearly on the inverse film thickness H. This is expected for small chains (having a gyration radius $R_g \ll H$) assuming as the simplest phenomenological description the linear superposition

$$
\mathcal{A} \approx \frac{1}{H}[\mathcal{A}_0\,(H-W) + \mathcal{A}_s\,W]
$$
$$
= \mathcal{A}_0\left[1 - \frac{(1-\mathcal{A}_s/\mathcal{A}_0)W}{H}\right] \tag{3}
$$

of a bulk term $\mathcal{A}_0$ with a weight $H - W \approx H$ and a surface term $\mathcal{A}_s$ with a weight proportional to the surface width $W \ll H$ [68]. Even more generally, $\mathcal{A}$ may be written as an average (possibly nontrivially weighted [64]) over z-dependent contributions $\mathcal{A}(z)$ as done, e.g., for the glass transition temperature T_g [47,54,64] or the storage and loss moduli $G'(\omega)$ and $G''(\omega)$ [60]. The claimed $1/H$-correction, Eq. (3), has merely the advantage to be based on a simple and transparent idea. It may be seen as the leading contribution of a more general $1/H$-expansion [68]. We remind that other H-dependencies have been suggested [44,45,47] and fitted with some success [52–54,56].

E. Outline

The different configuration ensembles are characterized in Sec. II before we present our numerical results in Sec. III. We start with the characterization of the film thickness H and the glass transition temperature T_g (Sec. III A) and discuss then the affine and nonaffine contributions μ_A and μ_F to the shear modulus μ (Sec. III B). We turn in Sec. III C to the Δt-dependence of time-preaveraged fluctuations and demonstrate that the stationarity relation Eq. (2) holds for films. Using the Einstein-Helfand relation [14,23] we compute in Sec. III D the shear viscosity η for our highest temperatures. The TTS scaling of $\mu(\Delta t, T)$ will be presented in Sec. III E. We confirm in Sec. III F the TTS scaling for the directly determined shear-stress relaxation modulus $G(t)$. That $\mu(\Delta t)$ is statistically better behaved as $G(t)$ is demonstrated using the standard deviations $\delta\mu$ and δG discussed in Sec. III G. We conclude the paper in Sec. IV. The definitions of $\hat{\sigma}$ and $\hat{\mu}_A$ are given in Appendix A. The model Hamiltonian is described in Appendix B 1. Details concerning the time and ensemble averages used can be found in Appendix B 2. The difference of simple averages and fluctuations is stressed in Appendix B 3. Appendix C reminds briefly the derivation of the stationarity relation, Eq. (2), already presented elsewhere [9,11,14].

II. ALGORITHM AND ENSEMBLES

A. General simulation aspects

As in our earlier work [6,13,14] our results are obtained by means of MD simulation of a coarse-grained bead-spring model of Kremer-Grest type [25]. Details concerning the

TABLE I. Some properties at the glass transition for the bulk and for films of different lateral box sizes L ensemble-averaged over m independent configurations: glass transition temperature T_g, film thickness H, affine shear modulus μ_A, shear-stress fluctuation μ_F, shear modulus μ according to Eq. (1), radius of gyration R_g, end-to-end distance R_e [2], and ratio H/R_g. The bulk results have been obtained at an imposed average normal pressure $P = 0$ using cubic periodic boxes. As emphasized in Sec. III C, it is important to specify that μ_F and μ have been obtained for a sampling time $\Delta t = 10^4$.

Ensemble	L	m	T_g	H	μ_A	μ_F	μ	R_g	R_e	H/R_g
3D bulk	–	10	0.395	–	93.3	84.6	8.7	1.9	4.6	–
film 1	23.5	120	0.371	21.3	93.9	85.6	8.3	1.9	4.6	11.3
film 2	37.1	10	0.334	8.5	94.2	86.1	8.1	1.9	4.6	4.5
film 3	42	10	0.318	6.6	94.3	86.5	7.8	1.9	4.6	3.5
film 4	49	10	0.290	4.8	94.9	87.4	7.5	1.8	4.4	2.6

model Hamiltonian may be found in Appendix B 1. Albeit the crossing of chains is effectively impossible in this model, entanglement effects are irrelevant for our short monodisperse chains of length $N = 16$ considered and Rouse-type dynamics [2] is observed at high temperatures. We use a velocity-Verlet scheme [23] with time steps of length $\delta t_{MD} = 0.005$. Temperature is imposed by means of the Nosé-Hoover algorithm provided by LAMMPS [25]. Periodic boundary conditions [23] are used for all our ensembles.

B. Film ensembles

We study free-standing polymer films containing $M = 768$ chains. As sketched in Fig. 2, the films are suspended parallel to the (x, y) plane with the same lateral box size L in x and y directions. As may be seen from Table I, we simulate ensembles with either $L = 23.5$ (called "film 1"), $L = 37.1$ ("film 2"), $L = 42$ ("film 3"), or $L = 49$ ("film 4"). The smallest L corresponds to our thickest films on which the discussion will often focus. Ensemble averages over $m = 120$ independently quenched configurations are performed for film 1, much more than the $m = 10$ configurations considered for all other ensembles. The vertical box size L_z is chosen sufficiently large ($L_z \gg H$) to avoid any interaction in this direction. The instantaneous stress tensor [23] vanishes outside the films. While this implies for all z planes within the films that the average vertical normal stress must vanish [51], some of the tangential normal stresses must be finite. The surface tension Γ [23,51] would otherwise vanish and the film be unstable. Note that $\Gamma \approx 1.7$ at the glass transition for all systems studied. It decreases weakly with temperature, but remains of order unity for all films study. As clarified in Appendix A 2, it is thus generally not appropriate to neglect the surface tension contribution to the Born-Lamé coefficients of stable films [61].

C. Bulk ensembles

For comparison we simulate in addition 3D bulk ensembles of same chain length N and chain number M contained in cubic periodic boxes at an imposed average pressure $P = 0$.

While the trace of the stress tensor must thus vanish on average for each configuration of the ensemble, this does not mean that the vertical normal stress for each z plane must vanish. This only applies for the ensemble average over independent configurations. This may matter (at least in principle) below the glass transition where frozen out-of-equilibrium stresses appear [14]. The ensembles used for bulk and film systems are thus similar, but not exactly identical as it would have been the case by imposing a vanishing normal stress in the z direction at a constant linear box length L in x and y directions. As shown in Sec. III, this difference appears, however, not to matter: all film data extrapolates nicely to the bulk data (indicated by stars) if plotted as a function of $1/H$ and assuming that the bulk data corresponds formally to the limit $1/H = 0$.

D. Quench protocol and data sampling

As already pointed out (Sec. II B) we do not directly vary the film thickness H but rather impose the lateral box width L. We first equilibrate an ensemble of m independent films at $T = 0.7$. As shown in Sec. III A, this temperature is well above the glass transition temperature T_g of all systems. We then quench each configuration using a constant quench rate. Specifically, we impose $T(t) = 0.7 - 2 \times 10^{-5}t$. Fixing then a constant temperature each configuration is first tempered over a time interval $\Delta t_{\text{temp}} = 10^5$. The subsequent production runs are performed over $\Delta t_{\max} = 10^5$. The same quench and production protocols are used for films and 3D bulk systems. Details concerning the different types of averages sampled can be found in Appendix B 2 and B 3. See Table I for several properties obtained at the glass transition.

III. NUMERICAL RESULTS

A. Film thickness and glass transition temperature

A central parameter for the description of our films is the film thickness H. We determine H using a Gibbs dividing surface construction [56,69]. With $\rho_0 \equiv \rho(z \approx 0)$ being the midplane density of the density profile $\rho(z)$, this implies

$$H \equiv NM/\rho_0 L^2. \tag{4}$$

As seen for one example in the top inset of Fig. 4, $\rho(z)$ is always uniform and smooth around the midplane in agreement with the data presented in previous studies [58]. ρ_0 can thus be fitted to high precision and, hence, also H. Since ρ_0 is always very close to unity, varying only little with L, Eq. (4) implies that (to leading order) $H \sim 1/L^2$ changes very strongly with L.

We present in the main panel of Fig. 4 the film thickness as a function of temperature. As emphasized by the dashed and the solid lines, the film thickness H—and thus the film volume $V = L^2H$—decreases monotonically upon cooling with the two linear branches fitting reasonably the glass (dashed line) and the liquid (solid line) limits. The intercept (horizontal and vertical dashed lines) of both asymptotes allows to define the apparent glass transition temperature T_g and the film thickness H_g at the transition [58]. (See Ref. [14] for bulk systems.) The values are given in Table I.
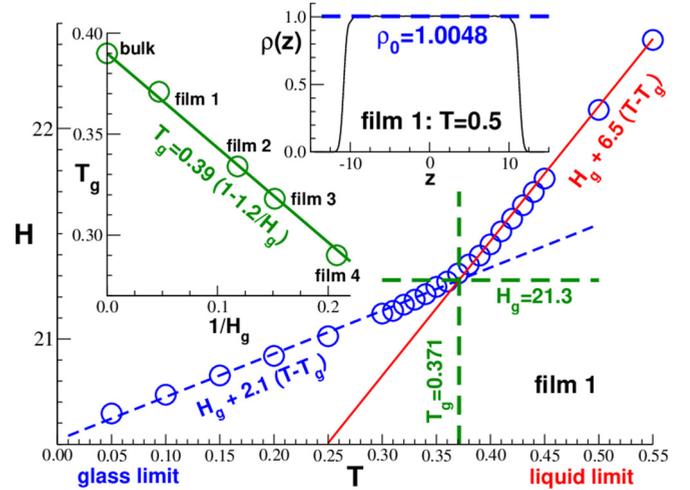

FIG. 4. Film thickness and glass transition temperature. Top inset: Number density profile $\rho(z)$ for $T = 0.5$ with $z = 0$ corresponding to the center of mass of each film. The midplane density $\rho_0 \approx 1$ is indicated by the dashed horizontal line. Main panel: H as a function of temperature T for film 1. The glass transition temperature T_g and the film thickness H_g at the transition (bold dashed lines) are operationally defined by the intercept of the linear extrapolations of the glass (dashed line) and liquid (solid line) limits. Left inset: T_g as a function of $1/H_g$ confirming the linear superposition, Eq. (3).

As expected from a wealth of literature [27–29,31,32,52–54,56–58,62], T_g increases with H. More precisely, as seen in the left inset of Fig. 4, T_g extrapolates linearly with the inverse film thickness to the thick-film limit. (The value $T_g = 0.395$ indicated at $1/H_g = 0$ stems from our bulk simulations.) This is consistent with a linear superposition, Eq. (3), of a thickness-independent bulk glass transition temperature T_{g0} and an effective surface temperature T_{gs} [68]. The negative sign of the correction implies $T_{gs} < T_{g0}$, i.e., surface relaxation processes are faster than processes around the film midplane. This is consistent with the higher monomer mobilities observed at the film surfaces [26,41,43,53,56,57,65]. We emphasize finally that many more data points covering a much broader range of orders of magnitude in $1/H$ are required to find or to rule out numerically higher orders of a systematic $1/H$-expansion of T_g.

B. Stress-fluctuation formula at constant Δt

Instantaneous values of the shear stress $\hat{\sigma}$ and of the affine shear modulus $\hat{\mu}_A$ have been computed as described in Appendix A 2. The time- and ensemble-averaged affine shear modulus $\mu_A \equiv \langle \overline{\hat{\mu}_A} \rangle$ is presented in Fig. 5 as a function of temperature using half-logarithmic coordinates. The averaged shear stress $\sigma \equiv \langle \overline{\hat{\sigma}} \rangle$ is not indicated since it vanishes rapidly due to symmetry with increasing ensemble size m and sampling time Δt. As seen from Fig. 5, this is not the case for the moments

$$\mu_0 \equiv \beta V \langle \overline{\hat{\sigma}^2} \rangle, \quad \mu_1 \equiv \beta V \langle \overline{\hat{\sigma}}^2 \rangle, \quad \mu_F \equiv \mu_0 - \mu_1 \tag{5}$$

(with $\beta = 1/T$ being the inverse temperature), describing the nonaffine contributions to the stress-fluctuation formula
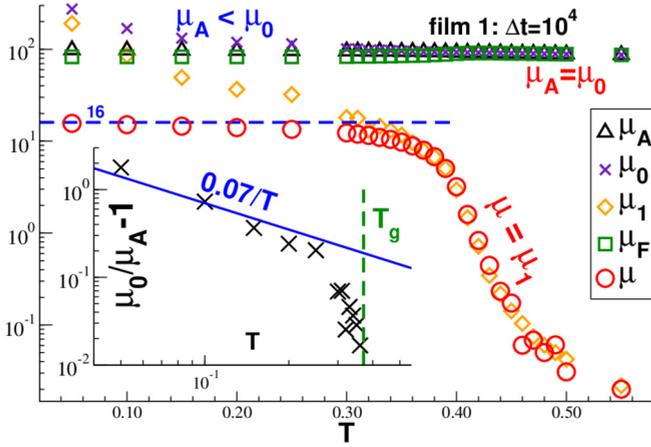
FIG. 5. Comparison of the different contributions to the shear modulus $\mu = \mu_A - \mu_F = (\mu_A - \mu_0) + \mu_1$ as functions of T focusing on data obtained for film 1 and $\Delta t = 10^4$. Inset: Double-logarithmic representation of $\mu_0/\mu_A - 1$ vs. T.

Eq. (1). Note that μ_F, μ_0, and μ_A depend only weakly on T and are all similar on the logarithmic scale used in Fig. 5.

As stressed elsewhere [14], $\mu_A = \mu_0$ for an equilibrium liquid since both $\mu = (\mu_A - \mu_0) + \mu_1$ and μ_1 must vanish. Frozen-in out-of-equilibrium stresses are observed upon cooling below T_g as made manifest by the dramatic increase of the dimensionless ratio $\mu_0/\mu_A - 1$. The β-prefactor of μ_0, Eq. (5), implies that due to the frozen stresses

$$\mu_0/\mu_A - 1 \sim 1/T \quad \text{for} \quad T \ll T_g \quad (6)$$

to leading order. This is consistent with the data presented in the inset of Fig. 5. Similar behavior has been reported for 3D polymer bulks [14].

Using a linear representation, the main panel of Fig. 6 presents $\mu_A(T)$ for all ensembles. This shows (more clearly than Fig. 5) that μ_A decreases continuously with temperature with two (approximately) linear branches in the glass and the liquid regimes as indicate by the two lines. While μ_A barely
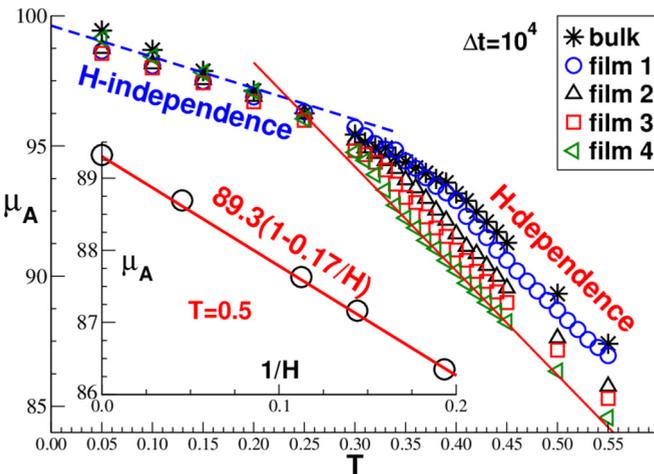

FIG. 6. Affine shear modulus μ_A. Main panel: $\mu_A(T)$ for all systems studied. Inset: As shown for $T = 0.5$, μ_A decreases linearly with $1/H$ in the liquid limit.
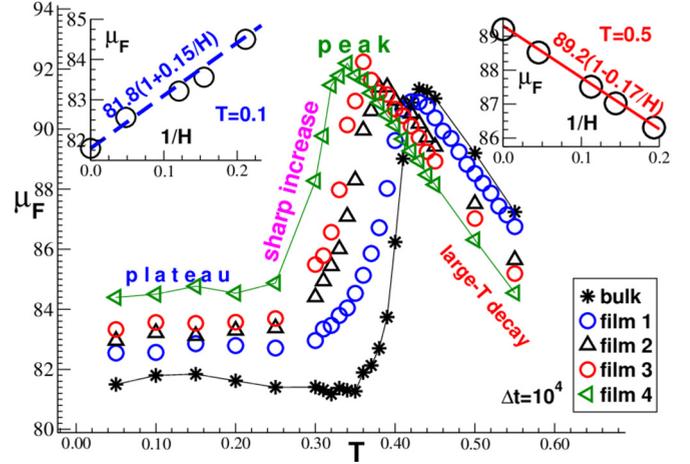

FIG. 7. Shear-stress fluctuation μ_F for $\Delta t = 10^4$. Main panel: $\mu_F(T)$ for all systems. Right inset: μ_F decreases linearly with $1/H$ in the liquid limit ($T = 0.5$). Left inset: μ_F increases linearly with $1/H$ in the solid limit ($T = 0.1$).

depends on H in the glass limit (suggesting a weak surface contribution μ_{As}), it increases with H in the liquid limit. As demonstrated in the inset, μ_A decreases in fact linearly with $1/H$ in agreement with Eq. (3) [70].

Using again a linear representation $\mu_F(T)$ is presented in the main panel of Fig. 7. Upon cooling it increases first (essentially linearly), goes through a well-defined peak located around T_g and drops then rapidly albeit continuously. It becomes constant for $T \ll T_g$ when the shear stresses get quenched. Since $\mu_A \approx \mu_F$ at high temperatures, the same linear $1/H$-dependencies are naturally observed as shown in the right inset of Fig. 7 for $T = 0.5$. At variance to this, μ_F *increases* linearly with $1/H$ at low temperatures as seen for $T = 0.1$ in the left inset, i.e., the nonaffine contributions are the largest for our thinnest films. Both linear $1/H$-relations for μ_F are consistent with Eq. (3). The negative sign of the correction for large T suggests that the bulk value μ_{F0} in the middle of the films must exceed the value μ_{Fs} at the surfaces while the opposite behavior occurs in the low-T limit [71].

As already highlighted in the main panel of Fig. 3, the shear modulus μ depends on the film thickness just as its affine (Fig. 6) and nonaffine (Fig. 7) contributions. Focusing on $\mu(T)$ it is shown in the main panel of Fig. 8 that these properties can be brought to collapse on H-independent mastercurves. The horizontal axis is rescaled with the reduced temperature T/T_g using the apparent glass transition temperature T_g defined in Sec. III A. The values $\mu_g \equiv \mu(T_g)$ used to make the vertical axes dimensionless are indicated in Table I and plotted in the inset of Fig. 8. Consistently with the linear superposition relation, μ_g is a linear function of $1/H_g$. Similar scaling plots could be given for the contributions $\mu_A(T)$, $\mu_0(T)$, $\mu_1(T)$, and $\mu_F(T)$.

C. Effective time-translational invariance

All data presented in the previous subsection have been obtained for one sampling time $\Delta t = 10^4$. We turn now to the characterization of the Δt-effects observed for μ in the inset of Fig. 3. Focusing on one temperature ($T = 0.3$) in the
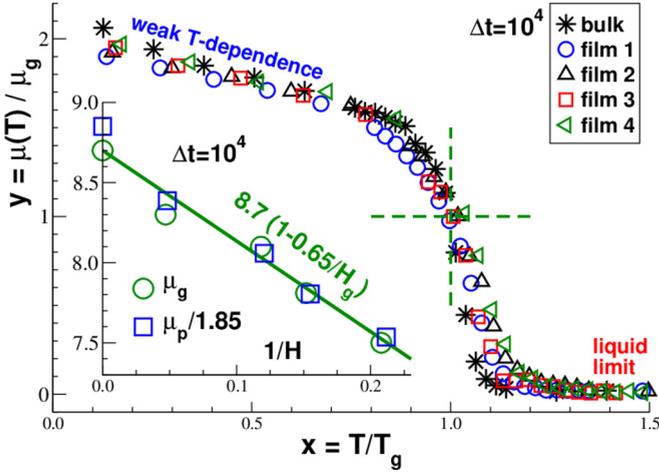
FIG. 8. Film thickness dependence of $\mu(T)$ for $\Delta t = 10^4$. Main panel: Scaling collapse of $y = \mu(T)/\mu_g$ vs $x = T/T_g$. Inset: $\mu_g \equiv \mu(T_g)$ and $\mu_p \equiv \mu(T = 0.1)$ vs. the inverse film thickness $1/H$ of the respective temperature. As emphasized by the bold line, both shear moduli are consistent with Eq. (3). We shall use μ_p in Secs. III E and III F for the TTS scaling of $\mu(\Delta t)$ and $G(t)$ comparing different ensembles.

glass limit, we compare in Fig. 9 the Δt-dependencies of μ_A, μ_0, μ_1, μ_F, and μ. As expected from Eq. (B8), the simple averages μ_A and μ_0 are found to be strictly Δt-independent. Importantly, time and ensemble averages do not commute for μ_1 since

$$0 = \beta V \overline{\langle \hat{\sigma} \rangle^2} < \beta V \overline{\langle \hat{\sigma}^2 \rangle} \equiv \mu_1(\Delta t), \qquad (7)$$

i.e., μ_1 is not a simple average but a fluctuation. As seen in Fig. 9, $\mu_1(\Delta t)$ decays in fact monotonically and, as a consequence, $\mu_F(\Delta t) = \mu_0 - \mu_1(\Delta t)$ increases and $\mu(\Delta t) = (\mu_A - \mu_0) + \mu_1(\Delta t)$ decreases monotonically. Interestingly, as indicated by the thin solid line, the stationarity relation Eq. (2) holds, i.e., $\mu(\Delta t)$ can be traced back from the
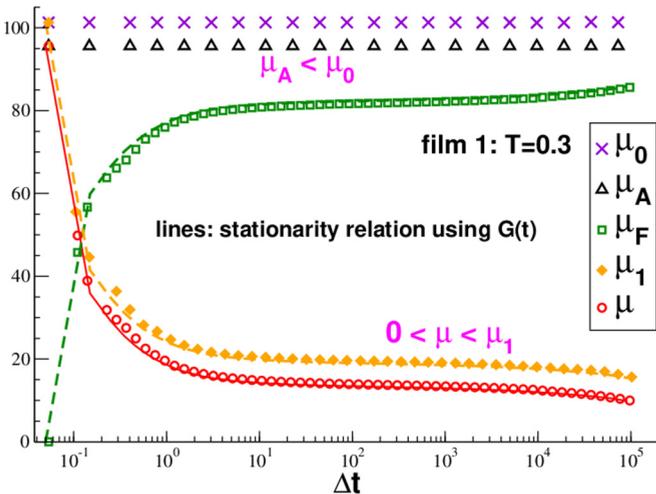

FIG. 9. Sampling time effects for μ and its contributions focusing on film 1 and $T = 0.3$. Only the simple averages μ_A and μ_0 are strictly Δt-independent. μ_1 and (hence) μ decrease monotonically. The solid and dashes lines have been obtained using Eq. (2).
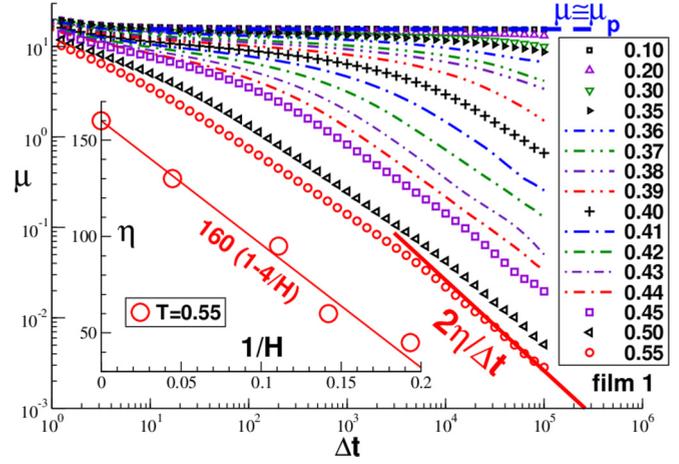

FIG. 10. Double-logarithmic representation of $\mu(\Delta t)$ for a broad range of temperatures T focusing on film 1. $\mu(\Delta t; T)$ decreases continuously with both Δt and T. A pseudoelastic plateau is observed in the solid limit with $\mu \approx \mu_p \approx 15.5$ (horizontal dashed line). The $1/\Delta t$-decay in the liquid limit (bold solid line) is expected from the Einstein-Helfand relation, Eq. (9). Inset: Shear viscosity $\eta(1/H)$ for $T = 0.55$. The values are used in Sec. III E to define an absolute scale for $\tau(T)$. The line presents a linear fit according to Eq. (3).

independently determined shear-stress relaxation modulus $G(t)$ discussed in Sec. III F. (The visible minor differences are due to numerical difficulties related to the finite time step and the inaccurate integration of the strongly oscillatory $G(t)$ at short times.) Since μ_A and μ_0 are Δt-independent simple averages, one can rewrite Eq. (2) to also describe $\mu_1(\Delta t)$ and $\mu_F(\Delta t)$. This is indicated by the two dashed lines. Note that Eq. (2) has been shown to hold for all temperatures and ensembles. The observed Δt-dependence of the shear modulus μ is thus not due to aging effects but arises naturally from the effective time-translational invariance of our systems. This does, of course, not mean that no aging occurs in our glassy systems but just that this is irrelevant for the timescales and the properties considered here. We shall now use the decay of $\mu(\Delta t) \approx \mu_1(\Delta t)$ for large T and Δt to characterize the shear viscosity $\eta(T)$.

D. Plateau modulus μ_p and shear viscosity η

That μ decreases monotonically with Δt is also seen in the main panel of Fig. 10 for a broad range of temperatures using a double-logarithmic representation. As already pointed out above (Fig. 3), it also decreases continuously with T and no indication of a jump singularity is observed. We emphasize that the same qualitative behavior is found for all systems we have investigated. (Similar plots have been obtained for glass-forming colloids in 2D [8] and for 3D polymers [13,14].)

As one expects, the Δt-dependence of μ becomes extremely weak in the solid limit, i.e., a plateau (shoulder) $\mu(\Delta t) \approx \mu_p = $ const appears for a broad Δt-window. Since the plateau value μ_p depends somewhat on T and on the Δt-window fitted, it is convenient for the dimensionless scaling plots presented in the next two subsections to define $\mu_p(H) \equiv \mu(T = 0.1, \Delta t = 10^4, H)$. The value for film 1 is indicated by the horizontal dashed line. As may be seen from the inset

of Fig. 8,

$$\mu_{\mathrm{p}}(H) \approx 16.1 \,(1 - 0.65/H) \approx 1.85\mu_{\mathrm{g}}(H), \qquad (8)$$

in agreement with Eq. (3).

As emphasized by the bold solid line in the main panel of Fig. 10, $\mu(\Delta t)$ decreases inversely with Δt in the high-T limit. This is expected from the Einstein-Helfand relation [14,23]

$$\mu(\Delta t) \to 2\eta/\Delta t \quad \text{for} \quad \Delta t \gg \tau, \qquad (9)$$

with η being the shear viscosity and τ the terminal shear stress relaxation time. Note that Eq. (9) follows directly from the stationarity relation Eq. (2) and the more familiar Green-Kubo relation $\eta = \int_0^\infty dt\, G(t)$ for the shear viscosity [2]. A technical point must be mentioned here. We remind that $\mu_{\mathrm{A}} = \mu_0$ in the liquid limit implies $\mu(\Delta t) = \mu_1(\Delta t)$. Since the impulsive corrections needed for the calculation of μ_{A} and, hence, of μ are not sufficiently precise for the logarithmic scale used here, it is for numerically reasons best to simply replace μ by μ_1 to avoid an artificial curvature of the data for large Δt. (See Fig. 16 of Ref. [14] for an illustration.) Using the Einstein-Helfand relation it is then possible to fit $\eta(T)$ above $T \approx 0.5$. For smaller temperatures this method only allows the estimation of lower bounds. (See the inset (b) of Fig. 17 of Ref. [14] for 3D bulks.) As shown in the inset of Fig. 10 for $T = 0.55$, the shear viscosity decreases systematically for thinner films and the linear superposition relation (solid line) describes reasonably all available data. We show now how $\eta(T)$ may be extrapolated to much smaller temperatures by means of the TTS scaling of $\mu(\Delta t)$.

E. Time-temperature superposition of $\mu(\Delta t)$

The TTS scaling of $\mu(\Delta t)$ is presented in the main panel of Fig. 11 using dimensionless coordinates and a double-logarithmic representation. Data for a broad range of temperatures are given for film 1 (open symbols) while we focus for clarity on one temperature ($T = 0.35$) for the other films (filled symbols) and the 3D bulk ensembles (stars). A good data collapse is achieved by plotting the rescaled shear modulus $y = \mu(\Delta t)/\mu_{\mathrm{p}}$ as a function of the reduced sampling time $x = \Delta t/\tau(T)$ using the relaxation time $\tau(T)$ indicated in the inset. The scaling function $y = f(x)$ is given by $f(x) \to \mathrm{const} \approx 1$ for $x \ll 1$ (dashed horizontal line) and by $f(x) \to 2/x$ for $x \gg 1$ (bold solid line) for consistency with the Einstein-Helfand relation. The vertical axis is made dimensionless using the plateau modulus μ_{p} introduced in Sec. III D. Please note that since according to Eq. (8) the H-dependence of μ_{p} is rather small on the logarithmic scales we are interested in, a similar good data collapse may also be achieved by simply setting $\mu_{\mathrm{p}} = 1$. Much more important is the rescaling of the horizontal axis by means of the terminal relaxation time $\tau(T, H)$ which depends strongly on both temperature and film thickness. Note that the strong H-dependence is masked by the rescaling of the horizontal axis using $x = T_{\mathrm{g}}(H)/T$ in the inset of Fig. 11.

Some remarks may be in order to explain how the scaling plot was achieved. We have in fact followed in a first step the standard prescription [1,2] fitting the relative dimensionless factors a_T and b_T for the horizontal and vertical rescaling
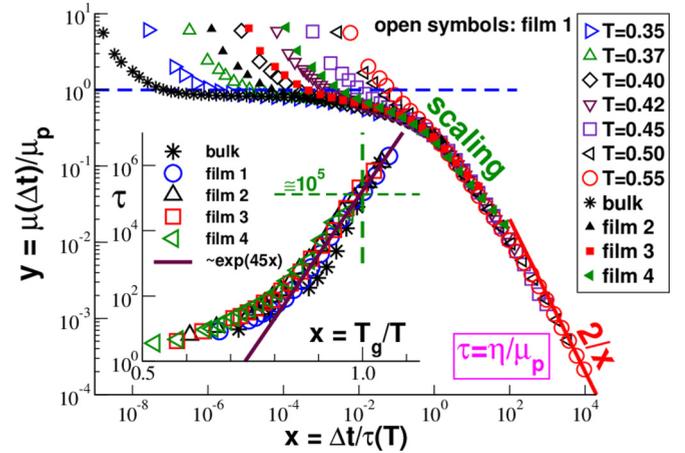

FIG. 11. TTS scaling for $y = \mu(\Delta t)/\mu_{\mathrm{p}}$ as a function of $x = \Delta t/\tau(T)$ with μ_{p} being the plateau modulus defined in Sec. III D and $\tau(T)$ the relaxation time indicated in the inset. We impose $\tau(T = 0.55)$ according to Eq. (10) to have an absolute timescale. The two asymptotics of the scaling function $y = f(x)$ for $x \ll 1$ and $x \gg 1$ are indicated by dashed and solid lines. Note the broad crossover regime between these limits. Inset: Data collapse of terminal relaxation time τ vs. $x = T_{\mathrm{g}}/T$ for all our ensembles. Arrhenius behavior (bold solid line) is observed around the glass transition ($x \approx 1$).

of $\mu(\Delta t, T)$ for temperatures T close to certain reference temperatures T_0. As one may expect [1], b_T can safely be set to unity for the entire temperature range we are interested in. In turn this justifies the temperature independent factor μ_{p} used to rescale the vertical axis. Naturally, merely tuning $a_T = \tau(T)/\tau(T_0)$ only sets the relative scale of $\tau(T)$. To fix the missing prefactor we impose

$$\tau(T) = c\,\eta(T)/\mu_{\mathrm{p}}(H) \quad \text{with} \quad c = 1 \qquad (10)$$

for $T = T_0 = 0.55$ using the shear viscosity η determined in the high-T limit by means of Eq. (9). Due to the somewhat arbitrary constant c/μ_{p} the strongest curvature of the rescaled shear modulus $y(x)$ coincides with $x \approx 1$. (Using instead $c \approx 100$ the crossover to the Einstein-Helfand decay would occur at about $x \approx 1$.) Consistency of $\mu(\Delta t) = \mu_{\mathrm{p}}f(x) \approx \mu_{\mathrm{p}}\tau/\Delta t$ for $x \gg 1$ and the Einstein-Helfand relation, Eq. (9), implies interestingly that Eq. (10) must hold for all temperatures. In other words, the relaxation time $\tau(T)$, shown in the inset of Fig. 11, and the shear viscosity $\eta(T)$ are equivalent up to a trivial prefactor. We emphasize that the stated proportionality hinges on the observation that $b_T \approx 1$.

As shown in the inset, a remarkable scaling collapse is achieved by plotting τ or η as a function of $x = T_{\mathrm{g}}/T$. Especially, this implies that we find

$$\tau(T \approx T_{\mathrm{g}}) = c\,\eta(T \approx T_{\mathrm{g}})/\mu_{\mathrm{p}}(H) \approx 10^5 \qquad (11)$$

for all our ensembles as shown by the horizontal and vertical dashed lines. In other words, the dilatometric criterion (Sec. III A) and the rheological criterion, fixing a characteristic viscosity for defining T_{g} [1], are numerically consistent on the logarithmic scales considered here. Anticipating better statistics and longer production runs (improving thus the precision of the TTS scaling), this suggests that Eq. (11) may

be used in the future to define T_g. We note finally that an Arrhenius behavior $\tau \sim \exp(45x)$ is observed for $x \approx 1$ (bold solid line) and that higher temperatures are consistent with a Vogel-Fulcher-Tammann law [1] (not shown).

F. Shear-stress relaxation modulus $G(t)$

While the (shear strain) creep compliance $J(t)$ [1] of polymer films has been obtained experimentally (by means of a biaxial strain experiment using effectively the reasonable approximation of a time-independent Poisson ratio near 1/2) [34,36,37,40], this seems not to be the case for the shear-stress relaxation modulus $G(t)$. This could in principle be done by suddenly tilting the frame on which a free-standing film is suspended and by measuring the shear stress $\sigma(t)$ needed to keep constant the tilt angle γ as shown in Fig. 1. The direct numerical computation of $G(t)$ by means of an out-of-equilibrium simulation tilting the simulation box in a similar manner, is a feasible procedure in principle as shown in Ref. [60]. For general technical reasons [23] this procedure remains tedious, however. (Being currently still limited to the high-frequency limit, it is especially not possible to get $G(t)$ by Fourier transformation of the storage and loss moduli $G'(\omega)$ and $G''(\omega)$ obtained by applying an oscillatory simple shear [60].) Fortunately, $G(t)$ can be computed "on the fly" using the stored time-series of $\hat{\sigma}$ and $\hat{\mu}_A$ by means of the appropriate linear-response fluctuation-dissipation relation. It is widely assumed [23] that $G(t)$ is given by the shear-stress autocorrelation function

$$c(t) \equiv \beta V \langle \overline{\hat{\sigma}(t)\hat{\sigma}(0)} \rangle. \tag{12}$$

However, as emphasized elsewhere [14], this expression can only be used under the condition that $\mu_A = \mu_0$. Albeit this does hold in the liquid limit of our films, as we have seen above (Fig. 5), this condition may not be satisfied below T_g [14]. It is thus necessary to obtain $G(t)$ below T_g using more generally [13,14]

$$G(t) = \mu_A - h(t) = (\mu_A - \mu_0) + c(t), \text{ with} \tag{13}$$

$$h(t) \equiv \frac{\beta V}{2} \overline{\langle (\hat{\sigma}(t) - \hat{\sigma}(0))^2 \rangle} = c(0) - c(t) \tag{14}$$

being the shear-stress mean-square displacement. Note that $G(t = 0) = \mu_A$ as it should if an affine strain is applied at $t = 0$ as sketched in Fig. 1(b).

Focusing on our thickest films and using a half-logarithmic representation, Fig. 12 presents $G(t)$ for all temperatures $T \leqslant 0.45$. Please note that albeit we ensemble-average over $m = 120$ independent configurations it was necessary for the clarity of the presentation to use in addition gliding averages over the total production runs, i.e., the statistics becomes worse for $t \to \Delta t_{\max} = 10^5$, and, in addition, to strongly bin the data logarithmically. Without this strong averaging the data would appear too noisy for temperatures around T_g. (See Sec. III G for a discussion of the standard deviation $\delta G(t)$ of $G(t)$.) However, it is clearly seen that $G(t)$ increases *continuously* with decreasing T without any indication of the suggested jump-singularity [16,17,19–21]. This is consistent with the continuous decay of the storage modulus $G'(\omega = const, T)$ as a function of temperature T shown in Fig. 6 of Ref. [60].
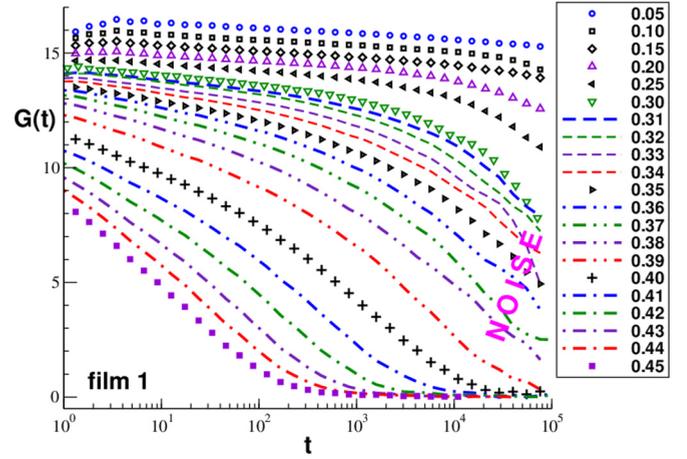

FIG. 12. Unscaled stress relaxation modulus $G(t)$ for film 1 using half-logarithmic coordinates. No indication of a jump singularity with respect to temperature is found.

Similar continuous behavior has also been reported for the Young modulus of polymer films [61].

Using a similar double-logarithmic representation as in Fig. 11, we demonstrate in Fig. 13 that a successful TTS scaling can be achieved for $G(t)$ just as for $\mu(\Delta t)$. While several temperatures are again indicated for film 1, only one temperature is indicated for the other ensembles. The effective power law -1 seen for $x \approx 1$ (solid line) can of course not correspond to the asymptotic long-time behavior since

$$\int_0^\infty dt\, G(t) = \eta \quad \text{and} \quad \int_0^\infty dt\, t\, G(t) = \tau \eta \tag{15}$$

would diverge. We remind that the Rouse behavior expected to hold for our short chains for large times corresponds to a cutoff with $y(x) \approx \exp(-x)/\sqrt{x}$ [2] for which all moments of $G(t)$ converge. Basically, due to the not accessible final cutoff it is yet impossible for any temperature $T \leqslant 0.55$ to determine
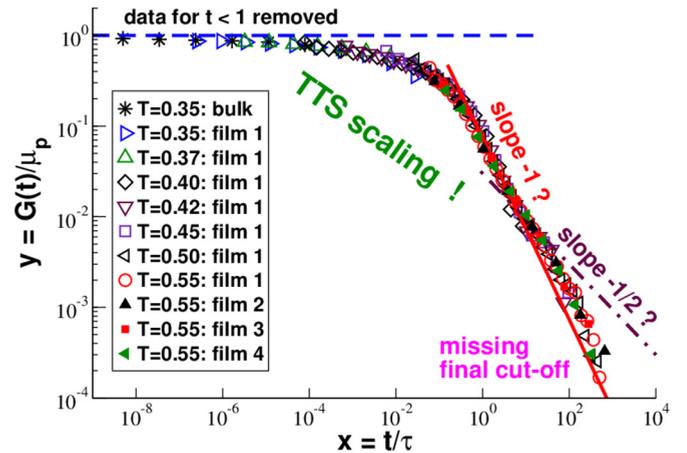

FIG. 13. Successful TTS scaling plot of $y = G(t)/\mu_p$ as a function of reduced time $x = t/\tau$ using the same relaxation times as in Fig. 11. The two indicated power laws (bold and dash-dotted lines) are given for comparison. Unfortunately, our production runs are too short to reveal the expected final exponential cutoff even for the highest temperatures.
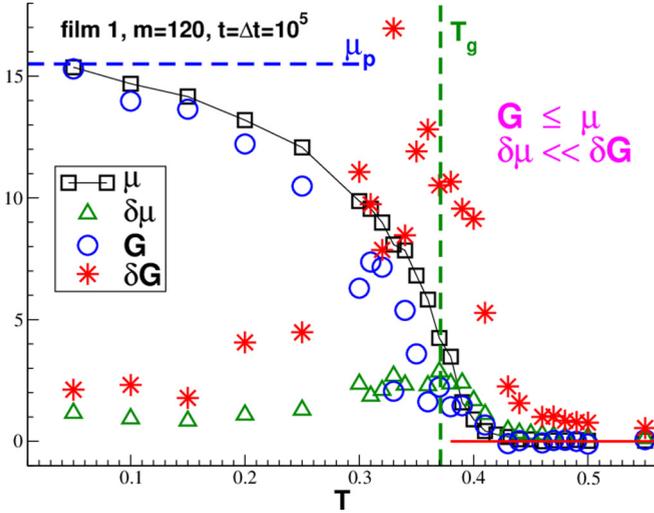
FIG. 14. Shear modulus μ, shear relaxation modulus G and the corresponding standard deviations $\delta\mu$ and δG taken at $t = \Delta t = \Delta t_{\max} = 10^5$ as functions of T. Focusing on film 1 all data are averaged over $m = 120$ configurations without additional gliding averages and logarithmic binning. The observed two inequalities $G \leqslant \mu$ and $\delta G \gg \delta\mu$ are both consequences of the stationarity relation Eq. (2).

η and τ merely by integrating $G(t)$, Eq. (15), and neither is it possible to compute $J(t)$ by Laplace transformation of $G(t)$ [1] in order to compare our numerical results with recent experiments [34,36,37,40]. It is mainly for this reason that we proceeded above by using the Einstein-Helfand relation and the TTS scaling of $\mu(\Delta t)$ to estimate η and τ. The unfortunate intermediate effective power-law slope -1 observed in Fig. 13 is presumably due to an intricate crossover between the exponential decay of the local glassy dynamics and the $1/\sqrt{x}$-decay (dash-dotted line) due to the chain connectivity. Albeit we do not expect any conceptional problems, much longer production runs are clearly warranted to clarify this issue.

G. Standard deviations $\delta\mu$ and δG

As already pointed out above, the data for $G(t)$ is quite noisy, especially around T_g, and we had to use gliding averages and a strong logarithmic binning for the clarity of the presentation. We want now to describe this qualitative observation in more quantitative terms. This is done in Fig. 14 (focusing again on film 1) where we compare μ and G and their respective standard deviations $\delta\mu$ and δG, Eq. (B6), taken at the same constant time $t = \Delta t = \Delta t_{\max} = 10^5$ and plotted as functions of the temperature T. (The corresponding error bars $\delta\mu/\sqrt{m-1}$ and $\delta G/\sqrt{m-1}$ are not shown.) While we still average over the m independent configurations, we do not use any gliding averaging or logarithmic binning.

As already presented in Fig. 3, $\mu(T)$ decreases both continuously and smoothly with T. Albeit $G(T)$ decreases also continuously, it reveals an erratic behavior for temperatures slightly below T_g (vertical dashed line). The inequality $G(T) \leqslant \mu(T)$ for all temperatures is expected from Eq. (C9). More importantly, being the second integral over $G(t)$, the

shear modulus μ automatically filters off the high-frequency noise. This explains the observed strong inequality $\delta\mu \ll \delta G$ of the standard deviations. At variance to μ and G, a striking nonmonotonic behavior is observed for $\delta\mu$ and δG with maxima slightly below the glass transition temperature T_g. While $\delta\mu \ll \mu$ and $\delta G \ll G$ in the solid limit, $\delta\mu > \mu$ and $\delta G > G$ at high and intermediate temperatures. It can be demonstrated that $\delta\mu/\mu \approx \sqrt{2}$ holds in this limit (as expected for general Gaussian fluctuating fields). Unfortunately, our statistics is insufficient to precisely quantify δG or $\delta G/G$. However, it should be clear from the presented data that the glass transition is masked—quite similar to what has been observed for 3D bulk systems [13,14]—by strong ensemble fluctuations with $\delta\mu/\mu$ and $\delta G/G$ of order of unity. The prediction of $G(T)$ or $\mu(T)$ for $T \approx T_g$ becomes thus meaningless for a single configuration. We emphasize finally that the inequalities $\delta\mu \ll \delta G$ and $\delta\mu/\mu \ll \delta G/G$ are the strongest slightly below T_g. This is the main reason why a numerical study of the elastic shear strain response around the glass transition should better focus on μ rather than of G.

IV. CONCLUSION

A. Methodology

Free-standing polymer films (Fig. 2) have been investigated by means of MD simulation of a standard coarse-grained polymer glass model (Appendix B 1). The film thickness $H \sim 1/L^2$ was tuned by varying the lateral box width L. The glass transition temperature T_g was obtained from the much weaker temperature dependence of H (Fig. 4). We have focused on the global in-plane shear stresses (Appendix A 2), their fluctuations (Sec. III B), and relaxation dynamics (Figs. 10–13). We used as the main diagnostic tool the first time-averaged and then ensemble-averaged (Appendix B 2) shear modulus μ and its various contributions as defined by the stress-fluctuation formula, Eq. (1).

B. Δt-dependence of μ and TTS scaling

As expected from previous work [10,13,14], μ decreases monotonically (Figs. 9–11) with the sampling time Δt. This Δt-dependence is perfectly described (Fig. 9) by the stationarity relation Eq. (2), i.e., the stress-fluctuation formula is equivalent to a second integral over the shear stress relaxation modulus $G(t)$. The crucial consequence from the computational perspective is that, filtering away the high-frequency noise, $\mu(\Delta t)$ is a natural smoothing function statistically much better behaved as $G(t)$. As shown from the standard deviations $\delta\mu$ and δG (Fig. 14), this is especially important for large times and for temperatures around the glass transition. While the shear viscosities η for the highest temperatures may be directly computed by means of the Einstein-Helfand relation for $\mu(\Delta t)$, Eq. (9), this is currently impossible using the corresponding Green-Kubo relation for $G(t)$, Eq. (15). Using the accurate TTS scaling of μ (Fig. 11) we are able to estimate $\eta(T) \sim \tau(T)$ for an even broader temperature range down to $\approx T_g$. The TTS scaling of $G(t)$ is then possible (Fig. 13) using the same rescaling parameters.

C. Continuous temperature behavior

In agreement with recent studies of 3D polymer glass-formers [13,14], μ and G are found to decrease both monotonically and continuously with temperature T (Figs. 3, 10–14). This result is qualitatively incompatible with mean-field theories [18–21] which find that the energy barriers for structural relaxation diverge at the glass transition causing the sudden arrest of liquid-like flow. Non-mean-field effects smearing out the transition are apparently crucial. The idea that correlations may matter around T_g is strongly supported by the remarkable peaks observed for the standard deviations $\delta\mu$ and δG (Fig. 14).

D. Film thickness effects

As expected assuming a linear superposition of bulk and surface properties, Eq. (3), the glass transition temperature T_g decreases linearly with $1/H$ (Fig. 4). Consistently, μ becomes finite at lower temperatures for thinner films (Fig. 3). The same linear superposition relation characterizes μ and its various contributions if taken in the low or high temperature limit (Figs. 6 and 7), the shear modulus μ_g at the glass transition and the plateau modulus μ_p (Fig. 8). Importantly, as shown in Figs. 11 and 13, it is possible to collapse $\mu(\Delta t)$ and $G(t)$ for all our ensembles using the strongly H-dependent relaxation time τ. (The weak H-dependence of the plateau modulus μ_p used for dimensionless reasons is less relevant for the scaling.) Moreover, since $\tau(T, H)$ is found to roughly scale as a function of the inverse reduced temperature $x = T_g(H)/T$ (Fig. 11), the H-dependencies of all standard viscoelastic properties [1] are essentially traced back to $T_g(H)$.

E. Discussion

While the shear viscosity and the terminal relaxation time at constant T are linear in $1/H$ for high temperatures (inset of Fig. 10) where τ is a weak function of x, for temperatures close to T_g this can only be the leading contribution of a more general $1/H$-expansion. Due to the strong x-dependence of $\tau(x)$ for $x \approx 1$ (Fig. 11), a weak variation of $1/H$ close to the glass transition must have a dramatic and in general nonlinear effect on the thickness dependence of various viscoelastic properties. As already pointed out elsewhere [54], some care is thus needed if $T_g(H)$ is operationally obtained by means of a rheological property other than Eq. (11). This may be an explanation for some of the $1/H$-expansions with higher order terms reported for $T_g(H)$ in the literature [64,66].

F. Outlook

We are currently investigating the z profiles of various properties considered here to confirm the superposition of bulk and surface properties and to demonstrate that Eq. (2) also holds for $\mu(\Delta t, z)$ and $G(t, z)$. The prefactor $c = 1$ used for the terminal relaxation time τ was somewhat arbitrary, Eq. (10). This was due to the missing exponential cutoff of $G(t)$ which made it impossible to determine τ accurately using Eq. (15) even for $T = 0.55$. We plan to do this at least for one high temperature using much longer production runs with $\Delta t_{\max} = 10^7$. Using these longer time series it should be possible to fit the Maxwell relaxation spectrum [1]. Together

with an improved TTS scaling of $G(t, T)$ this should allow us to obtain $G'(\omega, T)$ and $G''(\omega, T)$ and to compare our data with the experimentally available creep compliance $J(t, T)$ [34,36,37,40]. In addition we will attempt to characterize in more detail the scaling of the fluctuations between different configurations of the ensemble with the number of chains, the film volume, the film thickness and the sampling time. A quantitative theoretical theory describing the standard deviations $\delta\mu$ and δG, especially around T_g, is highly warranted.

APPENDIX A: INSTANTANEOUS PROPERTIES

1. Canonical affine transform

Let us consider an infinitesimal simple shear strain increment γ in the xy plane as it would be used to determine the shear relaxation modulus $G(t)$ by means of a direct out-of-equilibrium simulation (Sec. III F). For simplicity all particles are in the principal simulation box [23]. It is assumed [8] that all particle positions $\underline{r}$ and particle momenta $\underline{p}$ follow the imposed "macroscopic" strain in a *canonical affine* manner according to

$$r_x \rightarrow r_x + \gamma \, r_y \quad \text{and} \quad p_y \rightarrow p_y - \gamma \, p_x, \qquad (A1)$$

where the negative sign in the second transform assures that Liouville's theorem is satisfied. Please note that a general configuration will (except for very simple lattice systems) not follow an external macroscopic strain in an affine manner. The assumed transform is merely a theoretical trick [5,8].

2. Shear stress and affine shear modulus

The instantaneous shear stress $\hat{\sigma}$ and the instantaneous affine shear modulus $\hat{\mu}_A$ are defined by the first two functional derivatives [5,8,14]

$$\hat{\sigma} \equiv \left.\frac{\delta\hat{e}(\gamma)}{\delta\gamma}\right|_{\gamma=0} \quad \text{and} \quad \hat{\mu}_A \equiv \left.\frac{\delta^2\hat{e}(\gamma)}{\delta\gamma^2}\right|_{\gamma=0} \qquad (A2)$$

of the energy density $\hat{e} \equiv \hat{E}/V$ of the total energy $\hat{E}$ with respect to a canonical affine transform defined above. (We remind that for films $V = L^2 H$, with H being the film thickness defined in Sec. III A.) Assuming the energy $\hat{E} = \hat{E}_{id} + \hat{E}_{ex}$ to be the sum of an ideal and an excess contribution $\hat{E}_{id}$ and $\hat{E}_{ex}$, similar relations apply for the corresponding contributions $\hat{\sigma}_{id}$ and $\hat{\sigma}_{ex}$ to $\hat{\sigma} = \hat{\sigma}_{id} + \hat{\sigma}_{ex}$ and for the contributions $\hat{\mu}_{id}$ and $\hat{\mu}_{ex}$ to $\hat{\mu}_A = \hat{\mu}_{id} + \hat{\mu}_{ex}$. With $\hat{E}_{id} = \sum_{i=1}^{n} \underline{p}_i^2/2m$ being the standard kinetic energy for monodisperse particles of mass m, Eq. (A2) implies the ideal contributions

$$\hat{\sigma}_{id} = -\frac{1}{V}\sum_{i=1}^{n} p_{ix} p_{iy}/m \quad \text{and} \qquad (A3)$$

$$\hat{\mu}_{id} = \frac{1}{V}\sum_{i=1}^{n} \left(p_{ix}^2 + p_{iy}^2\right)/2m, \qquad (A4)$$

where the sums run over all n particles. Note that the minus sign for the ideal shear stress follows from the minus sign in Eq. (A1) required for a canonical transform. We have used a symmetric representation in Eq. (A4) exchanging x and y in Eq. (A1) and averaging over the equivalent canonical affine simple shear strains in x and y directions. Assuming a pairwise central conservative potential $\hat{E}_{\mathrm{ex}} = \sum_l u(r_l)$ with l labeling the interactions, r_l the distance between the pair of monomers and $u(r)$ a pair potential as defined in Appendix B 1, one obtains the excess contributions

$$\hat{\sigma}_{\mathrm{ex}} = \frac{1}{V} \sum_l r_l u'(r_l) \, n_{lx} n_{ly} \quad \text{and} \quad \text{(A5)}$$

$$\hat{\mu}_{\mathrm{ex}} = \frac{1}{V} \sum_l \left(r_l^2 u''(r_l) - r_l u'(r_l) \right) n_{lx}^2 n_{ly}^2$$

$$+ \frac{1}{V} \sum_l r_l u'(r_l) \left(n_{lx}^2 + n_{ly}^2 \right)/2, \quad \text{(A6)}$$

with $\underline{n}_l = \underline{r}_l / r_l$ being the normalized distance vector. As one expects, Eq. (A5) is strictly identical to the corresponding off-diagonal term of the Irving-Kirkwood stress tensor [23]. We have again used a symmetric representation for the last term in Eq. (A6). Importantly, this term takes into account the excess contribution of the normal tangential stresses in the (x, y) plane. These contributions cannot be neglected for stable films with finite surface tension. This last term corresponds to the well-known Birch coefficients [6,24] contributing to the elastic moduli of stressed systems. We also note that $\hat{\mu}_{\mathrm{ex}}$ depends on the second derivative $u''(r)$ of the pair potential. Impulsive corrections need to be taken into account due to this term if the first derivative $u'(r)$ of the potential is not continuous [7]. Unfortunately, this is the case at the cutoff of the shifted LJ potential, Eq. (B2), used in the current study.

APPENDIX B: COMPUTATIONAL DETAILS

1. Model Hamiltonian

All monomers that are not connected by bonds interact basically via a monodisperse LJ potential [23],

$$U_{\mathrm{LJ}}(r) = \epsilon_{\mathrm{LJ}}[(\sigma_{\mathrm{LJ}}/r)^{12} - (\sigma_{\mathrm{LJ}}/r)^6]. \quad \text{(B1)}$$

LJ units [23] are used throughout this work, i.e., the monomer mass m, the monomer diameter σ_{LJ}, the LJ energy parameter ϵ_{LJ} and Boltzmann's constant k_B are all set to unity. Length scales are given in units of σ_{LJ}, energies in units of ϵ_{LJ}, stresses and elastic moduli in units of $\epsilon_{\mathrm{LJ}}/\sigma_{\mathrm{LJ}}^3$ and times in units of $\sqrt{m\sigma_{\mathrm{LJ}}^2/\epsilon_{\mathrm{LJ}}}$. The LJ potential is truncated at $r_{\mathrm{cut}} = 2.3 \approx 2 r_{\mathrm{min}}$, with $r_{\mathrm{min}} = 2^{1/6}$ being the potential minimum, and shifted,

$$U_{\mathrm{LJ,trunc}}(r) = U_{\mathrm{LJ}}(r) - U_{\mathrm{LJ}}(r_{\mathrm{cut}}) \quad \text{for} \quad r \leqslant r_{\mathrm{cut}}, \quad \text{(B2)}$$

to make it continuous. It is, however, not continuous with respect to its first derivative and impulsive truncation corrections [24] are thus required for the determination of the Born-Lamé coefficients [7,8]. The flexible bonds are represented by the spring potential

$$U_{\mathrm{bond}}(r) = \frac{k_{\mathrm{bond}}}{2} \left(r - l_{\mathrm{bond}} \right)^2, \quad \text{(B3)}$$

with r being the distance between the permanently connected beads, $k_{\mathrm{bond}} = 1110$ the spring constant, and $l_{\mathrm{bond}} = 0.967$ the bond length.

2. Data sampling and averaging procedures

Instantaneous observables $\hat{a}$ are sampled every $10\delta t_{\mathrm{MD}}$ with $\delta t_{\mathrm{MD}} = 0.005$ being the time increment of the velocity-Verlet scheme used. Of central importance are the instantaneous shear stress $\hat{\sigma}$ and the instantaneous affine shear modulus $\hat{\mu}_A$ defined in Appendix A 2. Note that all intensive properties are normalized using the effective film volume $V = L^2 H$ with H being the film thickness defined in Sec. III A. As described in detail in Ref. [14], the stored time-series are used to compute for a given configuration various (arithmetic) *time averages* (marked by horizontal bars)

$$\overline{a} \equiv \frac{1}{i_2 - i_1 + 1} \sum_{i=i_1}^{i_2} \hat{a}_i, \quad \text{(B4)}$$

with $i = t/(10\delta t_{\mathrm{MD}})$ being the index of the time series and the sum running over all data entries of the time window $(t_1, t_2 = t_1 + \Delta t)$ with $\Delta t \leqslant \Delta t_{\mathrm{max}} = 10^5$ being the sampling time. By averaging over the m independent configurations, we obtain then *ensemble averages* (marked by pointy brackets)

$$\langle \mathcal{A}_j \rangle \equiv \frac{1}{m} \sum_{j=1}^{m} \mathcal{A}_j, \quad \text{(B5)}$$

with j being the configuration index and $\mathcal{A}_j$ some function of time preaveraged properties. The standard deviations $\delta\mu$ and δG discussed in Sec. III G are obtained using

$$\sqrt{\langle \mathcal{A}_j^2 \rangle - \langle \mathcal{A}_j \rangle^2} \quad \text{with} \quad \mathcal{A}_j = \overline{\mu} \quad \text{or} \quad = \overline{G}, \quad \text{(B6)}$$

being, respectively, the shear modulus or the relaxation modulus for a given time-window of a configuration. Essentially, the same data averaging procedure is used for the bulk systems the only difference being that we average finally in addition over the three equivalent shear planes.

3. Simple averages and fluctuations

It is important to distinguish in a computation study between *"simple averages"* $\langle \overline{a} \rangle$ and *"fluctuations"* such as [10,14,23]

$$\langle \overline{a}^2 \rangle \quad \text{or} \quad \overline{\langle (\hat{a} - \overline{a})^2 \rangle} = \langle \overline{\hat{a}^2} - \overline{a}^2 \rangle. \quad \text{(B7)}$$

It is well known that simple averages and fluctuations behave differently under ensemble transformation [10,23]. Incidentally, using the Lebowitz-Percus-Verlet transformation rules this provides one way to elegantly demonstrate the stress-fluctuation formula Eq. (1) within a couple of lines [8,10]. Interestingly, the expectation values, i.e., the ensemble averages for large m, of simple averages do not depend on the sampling time Δt since their time and ensemble averages commute [10,14]

$$\langle \overline{a} \rangle = \overline{\langle a \rangle} \sim \Delta t^0 \text{ since } \langle \hat{a} \rangle \sim \Delta t^0. \quad \text{(B8)}$$

As emphasized in Sec. III C, this does not hold in general for fluctuations. As reminded in Appendix C, it is always possible

for stationary systems to describe the Δt-dependence of time-preaveraged fluctuations in terms of a weighted integral over a corresponding correlation function. The specific relation relevant for the present work is given by Eq. (2).

APPENDIX C: FLUCTUATIONS IN STATIONARY TIME SERIES

1. Time-translational invariance

Let us consider a time series $(x_1, \ldots, x_n, \ldots x_N)$ with entries x_n sampled at equidistant time intervals dt. The time-averaged variance of this time series may be rewritten as

$$\overline{x^2} - \overline{x}^2 = \overline{(x_n - \overline{x})^2} = \frac{1}{2N^2} \sum_{n,m=1} (x_n - x_m)^2$$

$$= \frac{2}{N^2} \sum_{s=0}^{N-1} (N - s) \, \overline{h}(s, N), \qquad (C1)$$

using the in general s- and N-dependent sum

$$\overline{h}(s, N) \equiv \frac{1}{2} \frac{1}{N - s} \sum_{n=1}^{N-s} (x_{n+s} - x_n)^2. \qquad (C2)$$

If time-translational invariance can be assumed on average, we can readily take the expectation value $\langle \ldots \rangle$ over an ensemble of such time series. This yields

$$\langle \overline{x^2} - \overline{x}^2 \rangle = \frac{2}{N^2} \sum_{s=0}^{N-1} (N - s) \, h(s), \quad \text{with} \qquad (C3)$$

$$h(s) \equiv \langle \overline{h}(s, N) \rangle = c(0) - c(t) \quad \text{and} \qquad (C4)$$

$$c(s) \equiv \langle \overline{x_s x_0} \rangle. \qquad (C5)$$

Note that the mean-square displacement $h(s)$ and the correlation function $c(s)$ do only depend on the time-increment s for stationary time series.

2. Continuum limit

Using that the time series have been sampled with equidistant time steps, i.e., $t \approx s\,dt$ and $\Delta t \approx N\,dt$, the latter result becomes in the continuum limit

$$\langle \overline{x^2} - \overline{x}^2 \rangle = \mathcal{P}_{\Delta t}[h(t)] = c(0) - \mathcal{P}_{\Delta t}[c(t)], \qquad (C6)$$

where we have used the useful linear functional

$$\mathcal{P}_{\Delta t}[y(t)] \equiv \frac{2}{\Delta t^2} \int_0^{\Delta t} dt \, (\Delta t - t) \, y(t) \qquad (C7)$$

$$= \frac{2}{\Delta t^2} \int_0^{\Delta t} dt \int_0^t dt' \, y(t'). \qquad (C8)$$

Note that contributions at the lower boundary of the integral have a strong weight due to the $(\Delta t - t)$-factor in Eq. (C7). If $c(t)$ is a strictly monotonically decreasing function, this implies the inequality

$$c(t = \Delta t) < \mathcal{P}_{\Delta t}[c(t)]. \qquad (C9)$$

3. Back to current problem

Setting $x(t) \equiv \sqrt{\beta V} \hat{\sigma}(t)$ and assuming time-translational invariance for the sampled instantaneous shear stresses $\hat{\sigma}$, Eqs. (C6) and (14) lead to

$$\mu_{\mathrm{F}}(\Delta t) \equiv \mu_0 - \mu_1(\Delta t) = \mathcal{P}_{\Delta t}[h(t)] \qquad (C10)$$

for the Δt-dependence of the shear-stress fluctuations. Since μ_{A} is a constant, Eq. (13) implies

$$\mu(\Delta t) \equiv \mu_{\mathrm{A}} - \mu_{\mathrm{F}}(\Delta t) = \mathcal{P}_{\Delta t}[G(t)]$$

$$= \frac{2}{\Delta t^2} \int_0^{\Delta t} dt \int_0^t dt' \, G(t'), \qquad (C11)$$

in agreement with Eq. (2) stated in the Introduction. If $G(t)$ approaches a final constant μ_{eq}, as sketched in Fig. 1(b), or a broad intermediate plateau, $\mu(\Delta t)$ must ultimately follow, however, more slowly being dominated by the short-time behavior of $G(t)$. We note finally that we might have also used $\mu(\Delta t) \equiv \mathcal{P}_{\Delta t}[G(t)]$ as the fundamental definition rather then the thermodynamically motivated stress-fluctuation formula, Eq. (1).

[1] J. D. Ferry, *Viscoelastic Properties of Polymers* (John Wiley & Sons, New York, 1980).

[2] M. Rubinstein and R. H. Colby, *Polymer Physics* (Oxford University Press, Oxford, 2003).

[3] D. R. Squire, A. C. Holt, and W. G. Hoover, Physica **42**, 388 (1969).

[4] J.-L. Barrat, J.-N. Roux, J.-P. Hansen, and M. L. Klein, Europhys. Lett. **7**, 707 (1988).

[5] J. F. Lutsko, J. Appl. Phys **64**, 1152 (1988).

[6] B. Schnell, H. Meyer, C. Fond, J. P. Wittmer, and J. Baschnagel, Eur. Phys. J. E **34**, 97 (2011).

[7] H. Xu, J. P. Wittmer, P. Polińska, and J. Baschnagel, Phys. Rev. E **86**, 046705 (2012).

[8] J. P. Wittmer, H. Xu, P. Polińska, F. Weysser, and J. Baschnagel, J. Chem. Phys. **138**, 12A533 (2013).

[9] J. P. Wittmer, H. Xu, and J. Baschnagel, Phys. Rev. E **91**, 022107 (2015).

[10] J. P. Wittmer, H. Xu, and J. Baschnagel, Phys. Rev. E **93**, 012103 (2016).

[11] J. P. Wittmer, I. Kriuchevskyi, A. Cavallo, H. Xu, and J. Baschnagel, Phys. Rev. E **93**, 062611 (2016).

[12] D. Li, H. Xu, and J. P. Wittmer, J. Phys.: Condens. Matter **28**, 045101 (2016).

[13] I. Kriuchevskyi, J. P. Wittmer, H. Meyer, and J. Baschnagel, Phys. Rev. Lett. **119**, 147802 (2017).

[14] I. Kriuchevskyi, J. P. Wittmer, H. Meyer, O. Benzerara, and J. Baschnagel, Phys. Rev. E **97**, 012502 (2018).

[15] The sampling time Δt is the time window over which observables are first time-averaged according to Eq. (B4) for a given configuration before an ensemble average over m independent

configurations is performed. Δt should not be confused with the waiting time for systems with strong aging effects [14].

[16] G. Szamel and E. Flenner, Phys. Rev. Lett. **107**, 105505 (2011).

[17] M. Ozawa, T. Kuroiwa, A. Ikeda, and K. Miyazaki, Phys. Rev. Lett. **109**, 205701 (2012).

[18] H. Yoshino, J. Chem. Phys. **136**, 214108 (2012).

[19] H. Yoshino and F. Zamponi, Phys. Rev. E **90**, 022302 (2014).

[20] C. L. Klix, F. Ebert, F. Weysser, M. Fuchs, G. Maret, and P. Keim, Phys. Rev. Lett. **109**, 178301 (2012).

[21] C. L. Klix, G. Maret, and P. Keim, Phys. Rev. X **5**, 041033 (2015).

[22] A. Zaccone and E. M. Terentjev, Phys. Rev. Lett. **110**, 178002 (2013).

[23] M. P. Allen and D. J. Tildesley, *Computer Simulation of Liquids*, 2nd ed. (Oxford University Press, Oxford, 2017).

[24] D. Frenkel and B. Smit, *Understanding Molecular Simulation— From Algorithms to Applications*, 2nd ed. (Academic Press, San Diego, 2002).

[25] S. J. Plimpton, J. Comp. Phys. **117**, 1 (1995).

[26] T. Kajiyama, K. Tanaka, and A. Takahara, Macromolecules **28**, 3482 (1995).

[27] J. A. Forrest, K. Dalnoki-Veress, J. R. Stevens, and J. R. Dutcher, Phys. Rev. Lett. **77**, 2002 (1996).

[28] J. Mattsson, J. A. Forrest, and L. Börjesson, Phys. Rev. E **62**, 5187 (2000).

[29] J. A. Forrest and K. Dalnoki-Veress, Adv. Colloid Interface Sci. **94**, 167 (2001).

[30] K. Dalnoki-Veress, J. A. Forrest, C. Murray, C. Gigault, and J. R. Dutcher, Phys. Rev. E **63**, 031801 (2001).

[31] O. Bäumchen, J. D. McGraw, J. A. Forrest, and K. Dalnoki-Veress, Phys. Rev. Lett. **109**, 055701 (2012).

[32] J. A. Forrest and K. Dalnoki-Veress, ACS Macro Lett. **3**, 310 (2014).

[33] S. Napolitano, D. Prevosto, M. Lucchesi, P. Pingue, M. D'Acunto, and P. Rolla, Langmuir **23**, 2103 (2007).

[34] P. A. O'Connell and G. B. McKenna, Science **307**, 1760 (2005).

[35] M. Alcoutlabi and G. B. McKenna, J. Phys.: Condens. Matter **17**, R461(R) (2005).

[36] P. A. O'Connell, S. A. Hutcheson, and G. B. McKenna J. Polym. Sci. Part B: Poly. Phys. **46**, 1952 (2008).

[37] P. Chapuis, P. C. Montgomery, F. Anstotz, A. Leong-Hoi, C. Gauthier, J. Baschnagel, G. Reiter, G. B. McKenna, and A. Rubin, Rev. Sci. Instrum. **88**, 093901 (2017).

[38] G. B. McKenna and S. L. Simon, Macromolecules **50**, 6333 (2017).

[39] C. J. Ellison and J. M. Torkelson, Nature Mat. **2**, 695 (2003).

[40] H. Bodiguel and C. Fretigny, Eur. Phys. J. E **19**, 185 (2006).

[41] Z. Yang, Y. Fujii, F. Lee, C.-H. Lam, and O. Tsui, Science **328**, 1676 (2010).

[42] J. E. Pye and C. B. Roth, Phys. Rev. Lett. **107**, 235701 (2011).

[43] C.-H. Lam and O. K. C. Tsui, Phys. Rev. E **88**, 042604 (2013).

[44] P.-G. de Gennes, Eur. Phys. J. E **2**, 201 (2000).

[45] S. Herminghaus, Eur. Phys. J. E **8**, 237 (2002).

[46] P. Z. Hanakata, J. F. Douglas, and F. W. Starr, Nat. Commun. **5**, 4163 (2014).

[47] S. Mirigian and K. S. Schweizer, J. Chem. Phys. **146**, 203301 (2017).

[48] S. Merabia, P. Sotta, and D. Long, Eur. Phys. J. E **15**, 189 (2004).

[49] A. Dequidt, D. R. Long, S. Merabia, and P. Sotta, in *Polymer Glasses*, edited by C. B. Roth (CRC Press, Taylor & Francis Group, 2016), pp. 301–354.

[50] S. T. Milner and J. E. G. Lipson, Macromolecules **43**, 9865 (2010).

[51] F. Varnik, J. Baschnagel, and K. Binder, J. Chem. Phys. **113**, 444 (2000).

[52] F. Varnik, J. Baschnagel, and K. Binder, Phys. Rev. E **65**, 021507 (2002).

[53] S. Peter, H. Meyer, and J. Baschnagel, J. Polym. Sci. B **44**, 2951 (2006).

[54] S. Peter, H. Meyer, J. Baschnagel, and R. Seemann, J. Phys.: Condens. Matter **19**, 205119 (2007).

[55] M. Solar, H. Meyer, C. Gauthier, C. Fond, O. Benzerara, R. Schirrer, and J. Baschnagel, Phys. Rev. E **85**, 021808 (2012).

[56] J. A. Torres, P. F. Nealey, and J. J. de Pablo, Phys. Rev. Lett. **85**, 3221 (2000).

[57] T. S. Jain and J. J. de Pablo, Macromolecules **35**, 2167 (2002).

[58] T. R. Böhme and J. J. de Pablo, J. Chem. Phys. **116**, 9939 (2002).

[59] K. van Workum and J. J. de Pablo, Nano Lett. **3**, 1405 (2003).

[60] K. Yoshimoto, T. S. Jain, P. F. Nealey, and J. J. de Pablo J. Chem. Phys. **122**, 144712 (2005).

[61] A. Shavit and R. A. Riggleman, Macromolecules **46**, 5044 (2013).

[62] R. J. Lang and D. S. Simmons, Macromolecules **46**, 9818 (2013).

[63] R. J. Lang, W. L. Merling, and D. S. Simmons, ACS Macro Lett. **3**, 758 (2014).

[64] J. H. Mangalara, M. E. Mackura, M. D. Marvin, and D. S. Simmons, J. Chem. Phys. **146**, 1229 (2017).

[65] J. Chowdhury, Y. Guo, Y. Wang, W. L. Merling, J. H. Mangalara, D. S. Simmons, and R. D. Pries, J. Phys. Chem. Lett. **8**, 1229 (2017).

[66] B. D. Vogt, J. Polymer Sci., Part B: Poly. Phys. **56**, 9 (2018).

[67] H. Yoon and G. B. McKenna, Macromolecules **50**, 9821 (2017).

[68] Layer models assuming the coexistence of typically one or two interfacial layers and an inner layer with distinct mobilities are an often invoked interpretation for the relaxation of confined glass-forming liquids [28,32,33,39,41].

[69] M. Plischke and B. Bergersen, *Equilibrium Statistical Physics* (World Scientific, Singapore, 1994).

[70] It can be shown that the z distribution $\mu_A(z)$ has a broad surface regime at high temperatures explaining thus the strong $1/H$-corrections, while it vanishes suddenly at the surfaces at low temperatures.

[71] The different signs of the correction can be explained from the qualitative different shapes of the z distribution $\mu_F(z)$ in both temperature limits. While $\mu_F(z)$ is monomodal at large T with a maximum at the film midplane, it becomes bimodal below T_g with a minimum at the film midplane and maxima close to the surfaces. The reason for this is basically that the monomer mobility remains high at the surfaces, i.e., $\mu_F(z)$ can approach $\mu_A(z)$ from below, while $\mu_F(z) \ll \mu_A(z)$ in the bulk phase. Details will be given elsewhere.